Pergamon

PII: S0022-4073(97)00235-5

J. Quant. Spectrosc. Radiat. Transfer Vol. 60, No. 4, pp. 559–571, 1998

Printed in Great Britain
0022-4073/98 $19.00 + 0.00

REMOTE SENSING OF THE MESOSPHERIC TEMPERATURE PROFILE FROM CLOSE-TO-NADIR OBSERVATIONS: DISCUSSION ABOUT THE CAPABILITIES OF THE 57.5–62.5 GHz FREQUENCY BAND AND THE 118.75 GHz SINGLE O_2 LINE

J. R. PARDO,†‡§¶ M. GÉRIN,‖ C. PRIGENT,†¶ J. CERNICHARO,††
G. ROCHARD‡‡ and P. BRUNEL‡‡

† DEMIRM/Observatoire de Paris-Meudon, 61 Avenue de l'Observatoire, 75014 Paris, France; ‖ Radioastronomie Millimétrique, URA336 du CNRS, ENS, 24 Rue Lhomond, 75005 Paris, France; †† CSIC, IEM, Dpto. Fisica Molecular, Serrano 123, E-28006 Madrid, Spain and ‡‡ Centre de Météorologie Spatiale, Météo-France, B.P. 147 F-22302 Lannion, France

(Received 12 May 1997)

Abstract—The new generation of atmospheric temperature sounders at frequencies around 60 GHz plan to include channels for scanning at altitudes above ~ 45 km (AMSU-C of NOAA and SSM/IS of DMSP). The thermal emission of O_2 at such altitudes is affected by the interaction of the permanent magnetic moment of O_2 in its ground electronic state $^3\Sigma$ with the Earth's magnetic field resulting in a Zeeman splitting of the rotational lines. This physical phenomenon is polarization dependent. Thus, the magnetic field makes the analysis of data coming from channels sensitive to it much more complicated than in the case of low atmospheric channels (temperature weighting functions peaking below ~ 45 km) around 60 GHz. This paper discusses the choice of frequencies and polarizations in the spin-rotation oxygen lines around 60 and 119 GHz to cover the goals of the future temperature sounders above ~ 45 km.

1. INTRODUCTION

The thermal emission of atmospheric O_2 at frequencies within its spin-rotation band between 50 and 70 GHz, and near the spectroscopically related 118.75 GHz resonance, viewed from the top of the atmosphere is used for passive sounding of the atmospheric temperature vertical profile (see Bommarito[1] and Fishbein et al[2]). A subset of oxygen lines, that reach the highest atmospheric opacities in the domain 50–70 GHz are listed in Table 1 together with their spectroscopic parameters. We should choose observation frequencies close to the center of one or several of these resonances ($\nu - \nu_c \leq 4$ MHz) in order to perform temperature soundings at altitudes above ~ 45 km as demonstrate temperature weighting functions calculations.

For this study, it is necessary to take into account the Zeeman substructure of the lines in the mesosphere due to the interaction between the Geomagnetic field and the permanent dipole moment of the O_2 molecule. This has been described in earlier works (see Refs. 4–8). The anisotropic and polarization dependent radiative transfer is described by means of 3×3 refractivity matrices and their projection onto the phase plane in the case of plane waves. Observational evidence of this effect has been reported by Pardo et al[7], Hartmann et al[9] and Sandor and Clancy.[10] Depending on the observing polarization the central parts of the O_2 resonances (typically $\pm$ 4 MHz) viewed from the top of the atmosphere present a different profile and provide information about temperature at

‡ Also at: Observatorio Astronómico Nacional, Campus Universitario-Apartado 1143, E-28800 Alcalá de Henares, Madrid, Spain.
§ To whom all the correspondence should be addressed.
¶ Present address: NASA-Goddard Institute for Space Studies, 2880 Broadway, New York, NY10025, U.S.A.

Table 1. Spin-rotation resonances of the $^{16}O_2$ molecule in the central region of the 60 GHz complex. (O_2 lines between 57.5 and 62.5 GHz)

N_J	$N'_{J'}$	ν_c (GHz)	Osc. Str.†	$E_{lower}(K)$
11_{11}	11_{10}	57.61249	0.229E+02	272.9
9_9	9_8	58.32388	0.189E+02	186.0
3_3	3_4	58.44658	0.671E+01	24.6
7_7	7_6	59.16421	0.148E+02	115.7
5_5	5_6	59.59098	0.108E+02	61.8
5_5	5_4	60.30606	0.107E+02	61.8
7_7	7_8	60.43478	0.149E+02	115.6
9_9	9_{10}	61.15056	0.189E+02	185.9
11_{11}	11_{12}	61.80016	0.229E+02	272.7
13_{13}	13_{14}	62.41123	0.269E+02	376.1
3_3	3_2	62.48626	0.654E+01	24.4
1_1	1_0	118.75033	0.200E+01	1.0

N: total angular momentum quantum number, J: pure rotational quantum number. † The oscillator strength is a non-dimensional quantum-mechanical parameter related to the transition dipole matrix element (see e.g. Ref. 3) that is used, together with E_{lower}, to calculate total line intensities.

different altitudes. The different capabilities of the O_2 lines between 57.5 and 62.5 GHz for remote sensing above $\sim$ 45 GHz at different polarizations will be discussed in this paper.

First (Sec. 2) we present the calculations that are the basis for our spectroscopic analysis. Detailed discussions are given in Sec. 3, and finally (Sec. 4) we report our conclusions and recommendations about the realignment of the present situation of frequency sharing in this band between active and passive services [already discussed in the World Radio-communications Conference of 1997 (WRC-97)].

2. CALCULATIONS

We will focus our analysis on the basis of double-band sounding channels with local oscillator frequency situated between two O_2 resonances where the opacity is the lowest, and an intermediate frequency chosen so that the center of each band is situated at a given distance from the center of the corresponding resonances (the same for both). This has been the principle when designing the high atmosphere temperature sounding channels for the *Advanced Microwave Sounding Unit* (AMSU-C) and the *Special Sensor Microwave/Image Sounder* (SSM/IS). Their characteristics are listed in Table 2. The discussion will be based on calculations of temperature weighting matrices at single frequencies near the resonances.

2.1. The model

Radiative transfer calculations in the Earth's atmosphere at frequencies close to O_2 resonances have been incorporated into the ATM software described in Pardo.[8] The theoretical basis of the model, based on previous theoretical works by Lenoir[4,5] and Tinkham and Strandberg,[12,13] are described in Ref. 7.

To summarize the main points related to the work we present here, let us consider a plane wave that propagates along the z direction through the atmosphere. The wave associated magnetic vector will be

$$H_{xy}(z) = \exp[-G_{xy}(z)]\, H_{xy}(0), \tag{1}$$

where G_{xy} is a (2×2) refractivity matrix restricted to the phase plane. From the magnetic and electric wave's vectors it is possible to calculate the energy flux along z by means of the hermitian part of the so-called power-spectrum coherency matrix (Ref. 15):

$$S_{ij}(v) = \langle E_{pi}(v)\, H_j^*(v) \rangle \tag{2}$$

where $E_{px} = -E_y$ and $E_{py} = E_x$. At millimetric wavelengths when we use both the Rayleigh–Jeans (R-J) and the Local Thermodynamic Equilibrium (LTE) approximations it is possible to linearly

Table 2. Proposed configurations by NOAA and DMSP (instruments: AMSU-C and SSM/IS respectively) for "high atmospheric" temperature sounding channels in the spin-rotation band of O_2 around 60 GHz

AMSU-C

Channel number	ν_c (GHz) (both bands)	$\Delta\nu$ (MHz)	Pol.
16	60.79267 ± 0.3539	± 1.5	LC+RC
17	60.79267 ± 0.3558	± 0.4	LC+RC
18	60.79267 ± 0.3569	± 0.25	LC+RC
19	60.79267 ± 0.3579	± 0.5	LC+RC
20	60.79267 ± 0.3589	± 0.25	LC+RC
21	60.79267 ± 0.3600	± 0.4	LC+RC

SSM/IS "high atmosphere"

Channel number	ν_c(GHz) (both bands)	$\Delta\nu$ (MHz)	Pol.
19	63.2832 ± 0.2853	—	H+V
20	60.7927 ± 0.3579	—	H+V
21	$60.7927 \pm 0.3579 \pm 0.002$	—	H+V
22	$60.7927 \pm 0.3579 \pm 0.0055$	—	H+V
23	$60.7927 \pm 0.3579 \pm 0.016$	—	H+V
24	$60.7927 \pm 0.3579 \pm 0.050$	—	H+V

relate the hermitian part of $S_{ij}(\nu)$ with a brightness temperature matrix and to show that the solution of the radiative transfer equation for a homogeneous layer of thickness Δz, characterized by a physical temperature T, a pressure P, gases densities ρ_i and a magnetic field $\boldsymbol{H}$, is

$$T_B(z_f, \nu) = e^{-A(\nu)\Delta z}\, T_B(z_i, \nu)\, e^{-A^{*T}(\nu)\Delta z} + T\,[I - e^{-2A(\nu)\Delta z}], \tag{3}$$

where T_B is that "Brightness Temperature Matrix" in the (2×2) phase plane, the diagonal elements of which have to be associated with the brightness temperature in each polarization (of two independent used as basis in the phase plane). $A(\nu) = [G(\nu) + G^{*T}(\nu)]/2$ is the hermitian part of $G(\nu)$, that contains the effect of $\boldsymbol{H}$, and ν is the frequency.

For radiative transfer in a multilayer atmosphere we use $T_B(z_f, \nu)$ as entry for the next layer ($T_B(z_{i+1}, \nu)$). At the end of the last layer we obtain the final $T_B(\nu)$. At the beginning of the first layer we have to introduce a background brightness temperature matrix. For our application, total opacities along the path are expected to be more than 100 dB (see Fig. 1). So, the calculations do not need to include any background brightness temperature matrix. Then, the solution of the radiative transfer at the end of the path can be obtained like this:

$$T_B(\nu) = \sum_{i=1}^{n_{layers}} W(i, \nu)\; T\left(z_i + \frac{\Delta z_i}{2}\right), \tag{4}$$

where

$$W(i, \nu) = P_i(\nu)\,[I - e^{-2A(z_i + \Delta z_i/2, \nu)\Delta z_i}]\, P_i^{*T}(\nu), \tag{5}$$

and

$$P_i(\nu) = e^{-A(n_{layers}, \nu)}\, e^{-A(n_{layers}-1, \nu)} \cdot \ldots \cdot e^{-A(i+1, \nu)}, \tag{6}$$

$W(i, \nu)$ [or $W(z, \nu)$ for a continuous spatial coordinate] is the Generalized Temperature Weighting Matrix that is the main object of our calculations in this paper; z_i, Δz_i are the beginning position and the thickness of layer i.

2.2. *Application*

We have performed radiative transfer calculations for each O_2 line of Table 1. All the calculations have been achieved for nadir views above the point [45°N/Greenwich Meridian] in order to make reliable comparisons. The Geomagnetic field vector is obtained from the *International Geomagnetic Reference Field* (*IGRF*) the empirical representation of the Earth's magnetic field core recommended

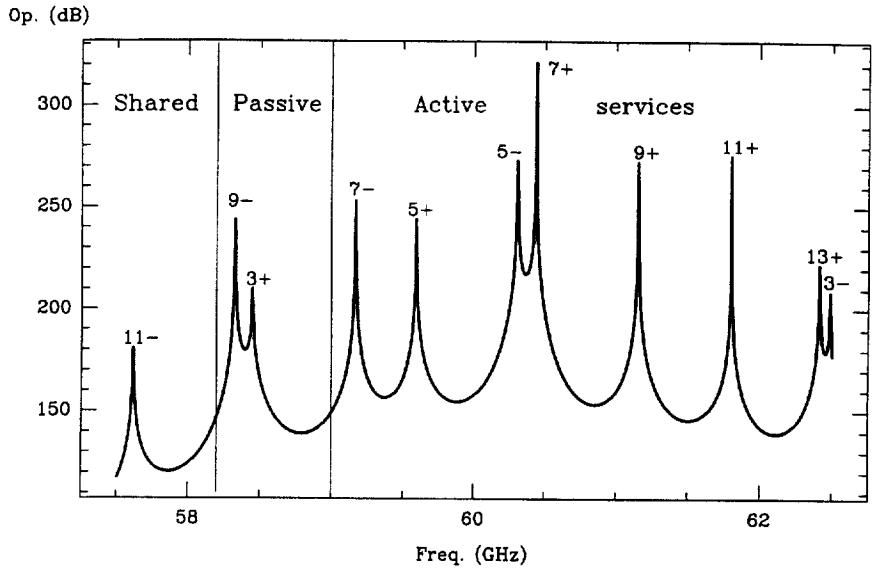

Fig. 1. Atmospheric zenith opacity (0 km– ∞) in the central part of the spin-rotation O_2 band (U.S. Stand. Atmospheric 1976,[11] and Liebe et al[6] absorption model). We have indicated the actual situation of frequency sharing between active and passive services in this band.

by the *International Association of Geomagnetism and Aeronomy* (*IAGA*) (see the work of Barraclough et al[14]). This model employs a spherical harmonics expansion of the scalar potential in geocentric coordinates. For this work we have taken the coefficient set corresponding to 1985. The validity of the conclusions given in this work is not affected by this choice. The atmospheric P/T vertical profile is the standard U.S. Stand. 1976 Atmosphere. Calculations are performed within ± 4 MHz around each single resonance with a spectral resolution between 20 and 50 kHz. The outputs of such calculations are brightness temperature and refractivity matrices in the phase plane (2×2) in two different polarization basis: (horizontal linear, vertical linear)† [thereafter noted (HL,VL)] as well as (left-hand circular, right-hand circular)† [thereafter noted (LC, RC)]. In all cases we have also calculated the temperature weighting matrices corresponding to the signal coming in each polarization. The following discussions are based on those calculations.

3. RESULTS AND DISCUSSION

In the first example we have taken the $N_J = 9_9 \rightarrow 9_{10}$ (9 +) O_2 line that was first chosen for the upper band of channels 16–21 of AMSU-C (see Table 2). The polarization must be RC or LC in order to get the highest sounding altitudes (the weighting function peaking at the highest altitude, see Fig. 2). Our calculations here show how the diagonal elements of the Temperature weighting matrices in a two-crossed linear polarization basis show double peaks and/or wide half-peak widths at frequencies placed between $\sim$ 0.2–1.5 MHz from the resonance (see Fig. 3). An additional channel is then necessary at the central frequency of a weaker O_2 line to fill the gap in the vertical coverage of the weighting functions when avoiding this $\sim 0.2 \text{ MHz} < |\nu - \nu_c| < \sim 1.5$ MHz region around the 7 + and 9 + resonances (weighting function that should peak at around 58–60 km in the case presented in Fig. 3). This is why SSM/IS channel 19th was proposed at the central frequencies of the 15 + and 17 + O_2 lines.

The problem of double-peaked weighting functions when observing in linear polarization near O_2 resonances from satellite needs a more careful analysis. We have performed calculations of

† At zenith view the horizontal and vertical linear polarizations are not well defined. So, we will call vertical linear the one following the direction of the unitary vector of the local meridian ($\boldsymbol{u}_\lambda$ in the phase plane) and horizontal linear the one following the direction of the local parallel unitary vector ($\boldsymbol{u}_\phi$ also in the phase plane).

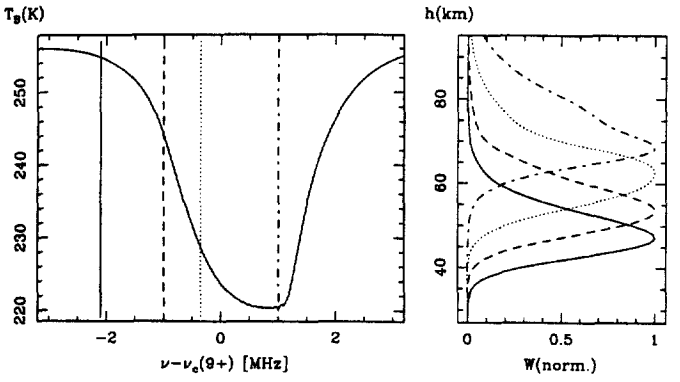

Fig. 2. Brightness temperature in LC polarization for satellite nadir view of the central part of the 9 + O_2 line above the geographic point [45°N/Greenwich Meridian] (U.S. Stand. Atmosphere, 1976). The right part of the figure displays the T-weighting functions corresponding to the four single frequencies indicated by means of different kinds of dotted/dashed/full lines in the left part of the figure. The highest weighting function peaks at 69 km. This picture can be associated to expected weighting functions of the AMSU-C channels (Table 3) at that geographical position.

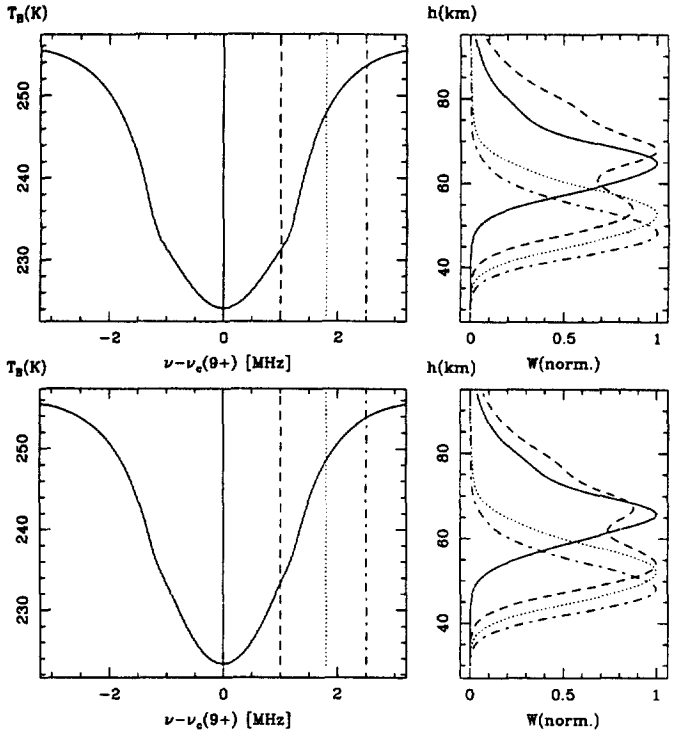

Fig. 3. The same as Fig. 2 but for HL (u_ϕ, upper part of the figure) and VL (u_λ, lower part) polarizations. Note the double-peaked weighting function corresponding to ν_c + 1 MHz.

temperature weighting matrices at equally spaced frequencies between 0.2 and 1.8 MHz from the center of the 7- and 9- O_2 resonances (ν_c = 59.16421 and 58.32388 GHz, respectively). The diagonal elements of those matrices have been normalized to unity at the altitude of the maximum at every single frequency. Then, "maps" (see Figs. 4 and 5) of these normalized elements are computed for different observing polarizations with respect to altitudes and frequencies: W(pol.,alt.,freq.). This representation, when superimposing the central position of the Zeeman components (for the mean value of the Geomagnetic field between 60 and 70 km of altitude), allows an interpretation of the degeneration of weighting functions at given frequencies and polarizations (see Figs. 4 and 5). The

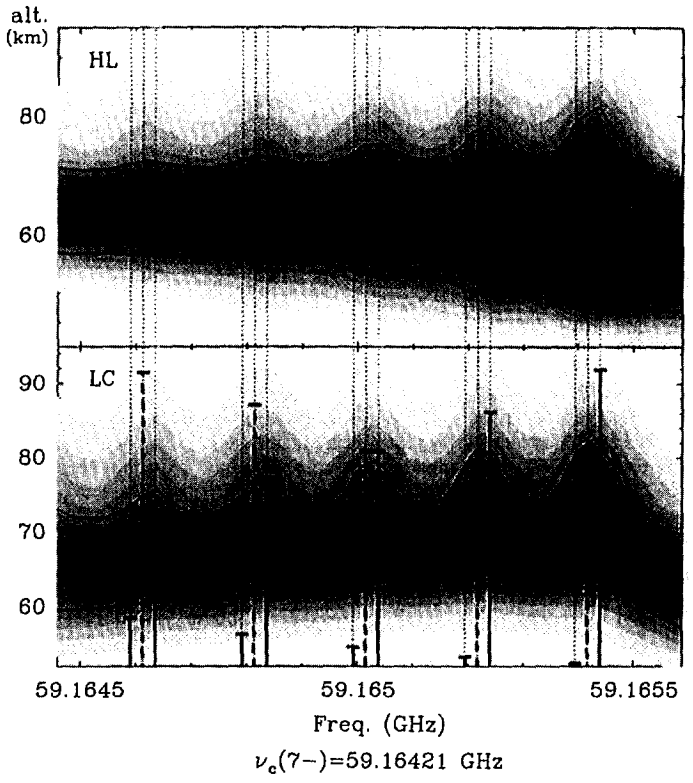

Fig. 4. Elements of the temperature weighting matrix associated to different observing polarizations (indicated in each box) at frequencies near the 7- resonance of O_2 for nadir view above [45°N/Greenwich Meridian]. Before representation, each diagonal element of the temperature weighting matrix corresponding to a single frequency has been normalized to unity at the altitude of its maximum. Thus, in the figure we have represented such elements as a function of altitude and frequency. We have superimposed to the maps the central positions of the Zeeman components for the mean value of the Earth's magnetic field between 50 and 70 km. The length of the thick bars represents the relative strengths of such components (dark bars: σ + components, grey bars: σ −, dashed bars: π components). The contour levels limiting the different grey zones run between 0 (clearest) to 0.9 with 0.1 steps. The 0.5 contour is given in order to see the vertical extent of the weighting functions at half-width. These "maps" are discussed in Section 3.

calculations show that weighting functions associated with observations in linear polarization have a larger half-peak width than the ones in circular polarization (RC or LC). This effect is specially important in the region between $\sim$ 0.5 and 1.5 MHz (or $-$ 0.5 and $-$ 1.5 MHz) from the unperturbed resonance (the central frequency of the line when there is no external magnetic field). The explanation of this fact appears in the figure: the Zeeman π components are distributed symmetrically around the unperturbed central frequency with decreasing relative line strengths with increasing distance between the components and this central frequency. On the other hand, the $\sigma \pm$ components show increasing line strengths with increasing distance of their position to the right or the left of the central frequency. So, when observing in linear polarization at, for example ν_c + 1.2 MHz, the receiver detects energy coming from linearly polarized emission of the π components but also part of the energy coming from strong σ components situated near that frequency (due to the projection of the circularly polarized emission into the observed linear polarization, see appendix A). The opposite is not true: when observing in circular polarization at the same frequency the receiver detects a much smaller amount of energy coming from the projection of the linearly polarized signal into the observed circular polarization due to the much weaker strengths of the π components near that frequency.

We have performed the same kind of calculations and analysis described above for each O_2 line between 57.5 and 62.5 GHz. The information about the position of the highest peaking weighting function corresponding to each line and each polarization is given in Table 3 (also for nadir view above [45°N/Greenwich meridian]). Also in the same table we give the "best" weighting function for

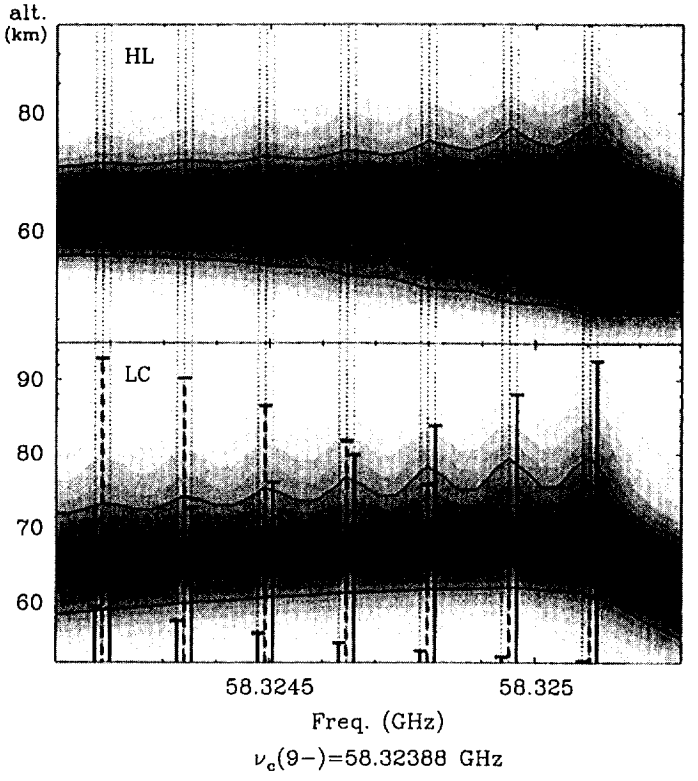

Fig. 5. The same as Fig. 4 (see explanation there) but for the 9- O_2 resonance centered at 58.32388 GHz.

each polarization, that means the one showing the best trade-off between the altitude of the peak (to be placed as high as possible) and the half-peak width (to be as narrow as possible).

One of the questions concerning the frequency sharing of the 57.5–62.5 GHz frequency band to be discussed during the WRC-97 is whether or not the passive services for atmospheric sounding have to keep the 60.3–61-3 GHz band for high-altitude measurements as described in the preliminary study for AMSU-C and SSM/IS channels (see Table 2). This band is at present exclusively attributed to active services. The band 58.2–59.0 GHz, exclusively attributed to passive services at present, gives in fact almost the same capabilities for the kind of soundings of concern here (see data about lines 7-, 9-, 7 + and 9 + in Table 3 and also the comparative plot in Fig. 6). The only objection made by the passive services is that the central frequency of the 7- O_2 resonance falls outside this band and it is necessary to built double side band channels similar to the ones specified in Table 2 for AMSU-C. So, we suggest to extend the protected frequency band for passive services up to 59.3 GHz. One objection could be: Why not just work with the 9- and 3 + resonances? From our calculations it appears that it is a need to take the 7- resonance because the pair (9-,7-) is closer spectroscopically (similar opacities and quantum numbers) than the pair (9-,3 +). That means that for the same frequency shift form the center of the 9- and 7- lines we are sounding at much closer altitudes than when we do the same with the 9- and 3 + resonances. Obviously, this makes much more easy the frequency choice for double side-band channels.

3.1. Capabilities of other O_2 lines

Our model allows to study the capabilities of other $^{16}O_2$ lines, or even isotopic O_2 lines, for this kind of temperature soundings. Obviously, the most interesting line outside the 50–70 GHz band is the 118.75 resonance. There are O_2 resonances at higher frequencies (in the submillimetric region) but they are spectroscopically different (see Pardo[8]) and such high frequencies have never been used for close-to-nadir view on meteorological systems. We will discuss here the 118.75 GHz O_2 line that

Table 3. Estimated maximum altitude of the peak of different diagonal elements of the Temperature weighting matrix, shift from the ν_c (Table 1) at which this maximum happens, and corresponding half-peak widths. Calculations have been performed for each oxygen line of Table 1 for nadir view above 45°N /Greenwich meridian. We give only calculations for LC polarization because the results for RC polarization are the same for the same frequency shifts but towards the lower frequencies with respect to ν_c. According to what we said in foot note †, we identify the direction of the local parallel (u_ϕ) with the horizontal linear polarization and the one of the local meridian (u_λ) with the vertical linear polarization

O_2 line	Pol.	Highest W			Best W		
		Alt. W peak	$\nu - \nu_c$ (MHZ)	Half-peak width (km)	Alt. W peak	$\nu - \nu_c$ (MHZ)	Half-peak width (km)
11-	LC	67–68	1.16	15	67–68	1.16	15.0
	u_ϕ	66–67	±1.04	26.4	63–64	±0.06	16.2
	u_λ	66–67	±1.04	27.0	64–65	±0.06	15.9
9-	LC	68–69	1.22	18.3	67–68	0.70	12.6
	u_λ	67–68	±1.08	29.6	65–66	±0.02	15.1
	u_ϕ	66–67	±1.08	29.5	65–66	±0.02	14.8
3+	LC	69–70	0.92	20.5	67–68	0.82	11.3
	u_λ	68–69	±0.94	38.5	63–64	±0.00	15.4
	u_ϕ	67–68	±0.78	27.6	65–66	±0.00	15.1
7-	LC	69–70	1.22	20.0	67–68	1.12	11.9
	u_λ	66–67	±1.04	34.8	65–66	±0.10	13.7
	u_ϕ	67–68	±1.04	28.8	65–66	±0.10	13.2
5+	LC	69–70	1.02	19.4	68–69	0.62	12.0
	u_λ	68–69	±1.04	36.4	65–66	±0.00	13.7
	u_ϕ	67–68	±0.70	26.3	66–67	±0.08	13.1
5-	LC	69–70	1.20	21.6	67–68	1.06	10.4
	u_λ	68–69	±1.20	37.2	65–66	±0.16	13.6
	u_ϕ	67–68	±1.16	32.9	65–66	±0.16	12.9
7+	LC	69–70	1.08	18.7	68–69	0.62	13.4
	u_λ	68–69	±0.96	32.6	65–66	±0.06	13.3
	u_ϕ	67–68	±0.90	28.5	65–66	±0.16	13.0
9+	LC	69–70	1.00	17.3	67–68	0.50	13.4
	u_λ	68–69	±1.02	31.9	65–66	±0.06	14.0
	u_ϕ	67–68	±0.90	29.6	66–67	±0.06	13.8
11+	LC	68–69	1.04	16.6	67–68	0.52	14.0
	u_λ	67–68	±1.06	31.2	65–66	±0.04	15.2
	u_ϕ	66–67	±0.92	28.4	65–66	±0.04	15.0
13+	LC	67–68	1.06	16.6	66–67	0.62	15.1
	u_λ	66–67	±1.08	30.8	61–62	±0.02	16.6
	u_ϕ	65–66	±0.90	28.1	63–64	±0.02	16.7
3-	LC	70–71	1.14	22.7	65–66	0.94	11.3
	u_λ	69–70	±1.16	38.8	63–64	±0.30	15.4
	u_ϕ	67–68	±1.10	34.9	63–64	±0.30	14.7

could be of interest in the near future. The higher frequency $^{16}O_2$ and $^{16}O^{18}O$ lines as well as the limb-sounding observing technique using O_2 lines will be discussed in a future work.

Some calculations are shown in Fig. 7. This shows first that the 118.75 GHz line allows to scan the mesospheric temperature ~ 5 km above the highest altitude allowed for frequencies in the range 57.5–62.5 GHz. However this is possible only in circular polarization and the observation in linear polarization shows a strong problem of double-peaked temperature weighting functions. In Appendix B we give some recommendations about the possible use of the 118.75 GHz line for the kind of observations considered here.

4. CONCLUSIONS AND RECOMMENDATIONS

The O_2 lines in the central part of the so-called 60 GHz complex are of great interest for temperature retrievals to be used for Numerical Weather Prediction (NWP) models. Together with the 118.75 GHz O_2 line, they are an unique resource for passive sounding at mesospheric altitudes. The actual situation of frequency sharing passive/active services in this band is not suitable for

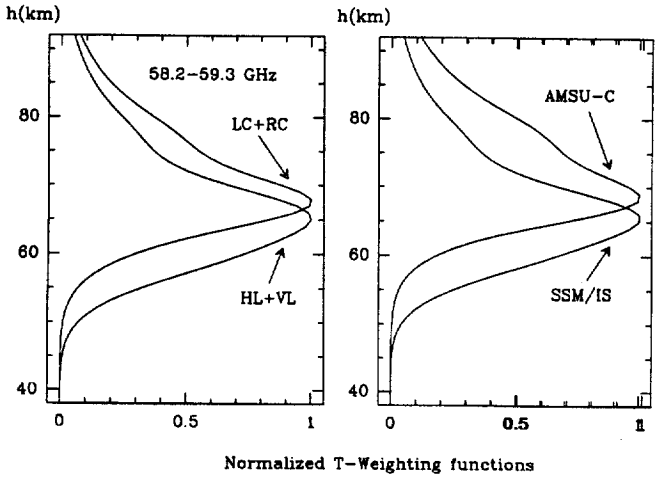

Fig. 6. This plot shows on the right the temperature weighting functions for the highest AMSU-C channel and the highest SSM/IS channel (both number 20 in their respective sections of Table 2) for nadir view over 45°N/Greenwich Meridian. They are compared (on the left) with the "best" possible weighting functions we can obtain by combining the 7- and 9- O_2 lines (that fall in the frequency band 58.2–59.3 GHz) for the same geographical position when observing in circular or linear polarization.

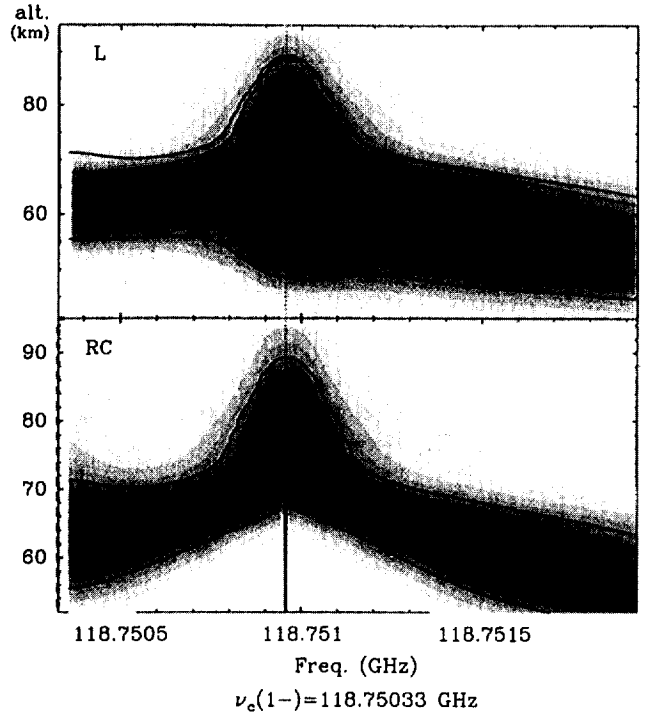

Fig. 7. Temperature weighting functions in linear and right-hand circular polarizations for satellite nadir view of the central part of the 1- O_2 line above the geographic point [45°N/Greenwich Meridian] (U.S. Stand. Atmosphere, 1976). The solid line indicates the half-peak width of the weighting functions at the different frequencies. You can clearly see the problem of double-peaks in the weighting functions corresponding to linear polarization. Observing in circular polarization allows to scan at higher altitudes at 118.75 GHz than at any frequency around 60 GHz. Note, however, that the position of the σ peaks will change with magnetic latitude. This problem is more critical for this line than for any O_2 line between 57.5 and 62.5 GHz. This is due to the presence of only 2 σ components at 118.75 GHz against at least more than 10 for lines between 57.5 and 62.5 GHz.

passive services since only two O_2 lines (9- and 3 +) fall into a band actually exclusively allocated to them. From the careful study presented in this paper we have to recommend the allocation of at least two neighboring O_2 resonances with similar quantum numbers for passive temperature sounding above $\sim$ 45 km. The more appropriate pairs of O_2 lines for this goal are (7+, 9+) or (7-, 9-). The (7+, 9+) pair was chosen for a preliminary study of the instruments AMSU-C (NOAA) and SSM/IS (DMSP). However, this pair is placed just in a frequency region of problematic sharing with active services. The second possibility (7-, 9-) is in a frequency range almost completely allocated at present to passive services (58.2–59.0 GHz) the only problem being that the central frequency of the 7- resonance is in fact 59.164 GHz. So, our recommendation is to allocate the band 58.2–59.3 GHz to passive services. In addition, the center of one or two lines below 58 GHz is necessary to fill the gap in the altitude coverage of weighting functions in linear polarization left by the non suitable (double-peaked) weighting functions at frequency shifts of the order of $\pm$ 0.3 to $\pm$ 1.5 MHz from the central frequencies (see Figs. 3–5). We suggest for this task to take the central frequencies of the 13- and 15- O_2 resonances (56.96822 and 56.36340 GHz). The frequency region 54.25 to 58.2 GHz is actually shared between passive and active services, so the conditions of this sharing should be carefully discussed due to the importance of this band for passive atmospheric sounding (because of the reason explained above and also due to the allocation of lower atmospheric channels, up to $\sim$ 45 km, of AMSU-A and SSM/IS as well as the systems MSU and SSM/T1).

We have to make a choice between linear polarization or circular polarization for the high atmospheric (up to $\sim$ 70–75 km) close-to-nadir observing instruments that we are considering here. A discussion of that point is given in Appendix B.

Acknowledgements—J. R. Pardo gratefully acknowledges the financial support of the Spanish *Ministerio de Educación y Ciencia*, the *Observatoire de Paris-Meudon*, *CNES* and *Météo-France* for the development of this work. He also recognizes the *NASA-Goddard Institute for Space Studies* for supplying him with computer and other facilities to achieve this work.

REFERENCES

1. Bommarito, J., Microvawe Instrumentation for Remote Sensing of the Earth, ed. C. Shine. *ISPIE Meeting, Orlando, FL*, April 1993.
2. Fishbein, E. F. et al, *J. Geophys. Res.*, 1996, **101**, 9983–10016.
3. Gordy, W. and Cook, R. L., *Microvawe Molecular Spectra*. Wiley, New York, 1984.
4. Lenoir, W. B., *J. Appl. Phys.*, 1967, **38**, 5283.
5. Lenoir, W. B., *J. Geophys. Res.*, 1968, **73**, 361–376.
6. Liebe, H. J. et al, Propagation modeling of moist air and suspended water/ice particles at frequencies below 1000 GHz. *Proc. AGARD 52nd meeting (Palma de Mallorca)*, 1993.
7. Pardo, J. R. et al, *J. Quant. Spectrosc. Radiat. Transfer*, 1995, **54**(6) 931.
8. Pardo, J. R., Thèse de Doctorat. Université Pierre et Marie Curie — Universidad Complutense de Madrid, 1996.
9. Hartmann, G. K. et al, *Geophys. Res. Lett.*, 1996, **23**, 2329.
10. Sandor, B. J. and Clancy, R. T., Mesospheric observations and modeling of the Zeeman split 233.9 GHz $^{18}O^{16}O$ line, *Geophys. Res. Lett.*, 1998, **24**(13), 1631.
11. U. S. Commitee On Extension to the Stnd. Atm., *U.S. Printing Office*, Washington D.C., 1976.
12. Tinkham, M. and Strandberg, M. W., *Phys. Rev.*, 1955, **97**, 937.
13. Tinkham, M. and Strandberg, M. W., *Phys. Rev.*, 1955, **97**, 951.
14. Barraclough, D. R., International geomagnetic reference field: the fourth generation, *Phys. Earth Planet. Inter.*, 1987, **48**, 279.
15. Born, M. and Wolf, E., *Principles of Optics*, 2nd edn., Pergamon Press, Oxford, 1964.
16. Rosenkranz, P. W. and Stealin, D. H., Polarized thermal microwave emission from oxygen in the mesosphere. *Radio Sci.*, 1988, **23**(5), 721–729.

APPENDIX A. DETECTION OF CIRCULARLY POLARIZED SIGNAL WHEN OBSERVING IN LINEAR POLARIZATION

The brightness temperature matrix of Eq. (3) should be expressed in the polarization basis (formed by two independent vectors) in the phase plane (we consider plane waves). Then, the diagonal elements of this matrix have to be associated to the brightness temperature to be detected when observing in the two polarizations described by the two complex vectors of the basis. The brightness temperature matrix can be written in any polarization basis. If Γ is the unitary matrix to transform the first basis $(\boldsymbol{u}_1, \boldsymbol{u}_2)$ into the second $(\boldsymbol{u}'_1, \boldsymbol{u}'_2)$ as shown:

$$\boldsymbol{u}'_1 = \Gamma_{11}\boldsymbol{u}_1 + \Gamma_{12}\boldsymbol{u}_2, \qquad \boldsymbol{u}'_2 = \Gamma_{21}\boldsymbol{u}_1 + \Gamma_{22}\boldsymbol{u}_2.$$

Then the brightness temperature matrix in the second basis will be

$$T'_B = \Gamma T_B \Gamma^{t*}.$$

If we start with a T_B described on the basis of two orthogonal linear polarizations [let us call them "horizontal" (LH) and "vertical" (LV)], the unitary matrix to transform to the right-circular (RC) and left-circular [LC] basis is:

$$\Gamma = \frac{1}{\sqrt{2}} \begin{pmatrix} 1 & -i \\ 1 & i \end{pmatrix}.$$

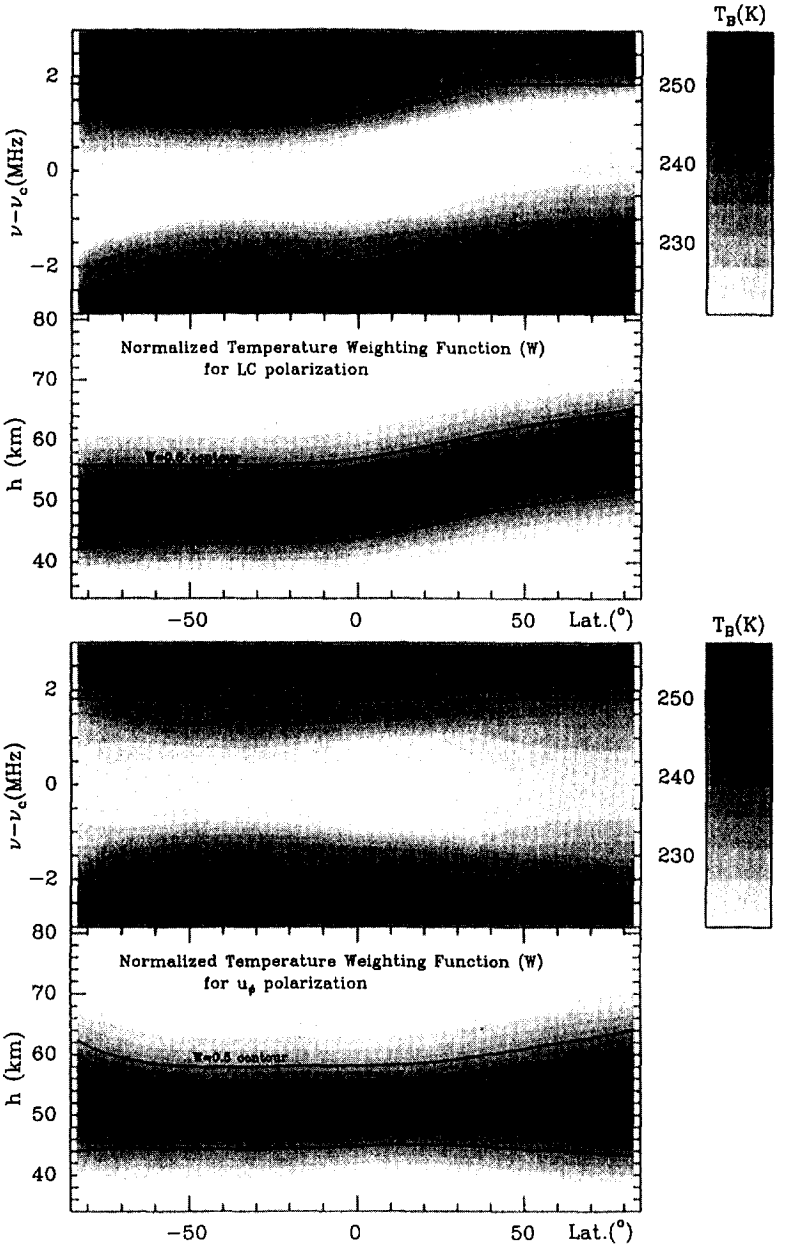

Fig. 8. Element (1,1) of the brightness temperature matrix around the 7- O_2 line and element (1,1) of the corresponding temperature weighting matrix (at $\nu - \nu_c = 1.9$ MHz) in two polarization basis [(LC, RC) and u_ϕ, u_λ)] represented as a function of latitude for nadir view over the Greenwich Meridian. The figure shows larger differences in latitude of the vertical position of the weighting functions at circular polarizations than at linear polarizations.

So, if we have a completely polarized right-hand + left-hand circularly radiation with brightness temperature matrix [in the (RC,LC) basis] equal to (elements given in K):

$$\begin{pmatrix} 240 & 0 \\ 0 & 280 \end{pmatrix}$$

it is easy to show that the corresponding brightness temperature matrix in the (HL,VL) basis is

$$\begin{pmatrix} 260 & i20 \\ -i20 & 260 \end{pmatrix}$$

that means we detect then a brightness temperature of 260 K when observing in HL or VL polarizations.

APPENDIX B. LINEAR OR CIRCULAR POLARIZATION?

This is a discussion about drawbacks and advantages of double side-band channels observing in linear or circular polarization:

I. From the technical point of view, the choice of circular polarization (first proposed by Rosenkranz and Stealin[16]) seems complicated because in order to get the signal from a similar atmospheric region it is necessary to detect right-hand circularly polarized radiation in one side-band and left-hand circularly polarized radiation in the other. Observing in linear polarization is much more simple: the same linear polarization for the two bands is fine, however there is a need to build a second receiver at the central frequencies of less opaque O_2 resonances in order to fill a gap in the vertical coverage of the weighting functions that appears when using only the 7- and 9- resonances (discussed above).

II. From the point of view of vertical coverage and resolution at a given geographical position it appears from Table 3 and Fig. 4 and 5 that it is better to use circular polarization than linear due to sensibility to higher altitudes with better vertical resolution.

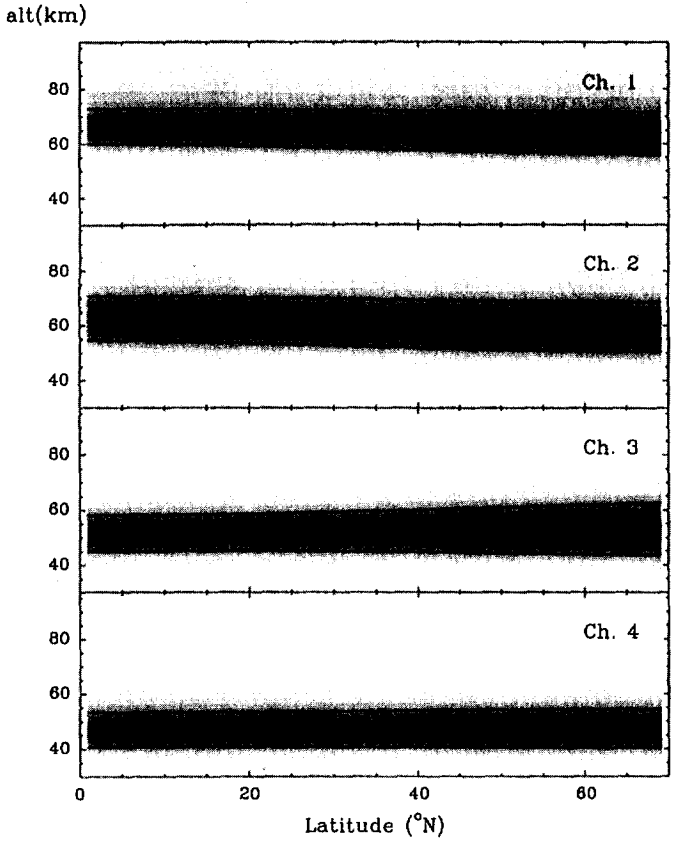

Fig. 9. Normalized (1,1) element of the temperature weighting matrix corresponding to linear polarization in the direction of the local parallel (u_ϕ) and nadir view at the central frequency of the upper band of the 4 channels defined in Table 4. This element has been represented in Fig. 4. The black contours correspond to the 0.5 level (half-peak).

Table 4. Proposed configuration for a close-to nadir view multichannel radiometer devoted to temperature sounding of the atmosphere from ~45 to 70 km. The frequency width of each individual channel is not given because it has to be fixed from sensibility criteria. It should be of the order of 0.2–0.5 MHz (then, the weighting functions will be broader but by less than 5%)

Channel ID (Fig. 9)	ν_{OL} (GHz)	ν_{IF} (GHz)	Pol.
1	58.74405	0.42016	Linear
2	56.66581	0.30241	Linear
3	58.74405	0.42206	Linear
4	58.74405	0.42316	Linear

III. From the point of view of systems to have global coverage, as it is the case when they are on board polar satellites at ~800 km of altitude (actual TIROS and DMSP), there is the problem of the changes with latitude of both the Geomagnetic field strength and its orientation with respect to the phase plane for channels sensitive to atmospheric altitudes where polarization effects become important in the radiative transfer. Our calculations show that latitude variations of the altitude domain where the weighting functions are above their half-peak are stronger for cirular polarizations than for linear polarizations (see Fig. 8). The linear polarization appears much better in this respect (Fig. 9). However, for the 118.75 GHz O_2 line the problem of double-peaked temperature weighting functions is critical in linear polarization whereas its simple Zeeman structure (only 3 components) makes it easier than for the other lines to take into account the variations of the mesospheric weighting functions for circular polarization with changing geographical position.

The conclusion is that double side-band channels with the characteristics given in Table 4 are the best choice in the range 57.5–62.5 for close-to-nadir view instruments with latitude coverage from ~70°S to ~70°N to perform temperature, soundings between ~45 to ~70 km of altitude, and taking into account the discussion about frequency sharing given above. A convenient design can be also found around the 118.75 GHz resonance using circular polarization due to the relatively simple Zeeman structure of this line.